Calculation of Optical Signal Using Three-Dimensional Bidomain/ Diffusion Model Reveals Distortion of the Transmembrane Potential

Phillip Prior and Bradley J. Roth
Department of Physics, Oakland University, Rochester, Michigan

ABSTRACT Optical mapping experiments allow investigators to view the effects of electrical currents on the transmembrane potential, V_m, as a shock is applied to the heart. One important consideration is whether the optical signal accurately represents V_m. We have combined the bidomain equations along with the photon diffusion equation to study the excitation and emission of photons during optical mapping of cardiac tissue. Our results show that this bidomain/diffusion model predicts an optical signal that is much smaller than V_m near a stimulating electrode, a result consistent with experimental observations. Yet, this model, which incorporates the effect of lateral averaging, also reveals an optical signal that overestimates V_m at distances >1 mm away from the electrode. Although V_m falls off with distance r from the electrode as $\exp(-r/\lambda)/r$, the optical signal decays as a simple exponential, $\exp(-r/\lambda)$. Moreover, regions of hyperpolarization adjacent to a cathode are emphasized in the optical signal compared to the region of depolarization under the cathode. Imaging methods utilizing optical mapping techniques will need to account for these distortions to accurately reconstruct V_m.

INTRODUCTION

An important question in cardiology is how an electric shock applied to the heart affects the transmembrane potential, V_m, during ventricular defibrillation (1). Over the last decade, the technique of optical mapping has allowed direct measurement of the transmembrane potential distribution during a shock (2,3). One limitation of optical mapping is that it does not measure the transmembrane potential at the tissue surface, but represents an average of the transmembrane potential over depth (4). Several experiments have examined the depth from which optical signals arise, but the results are inconsistent (5–8). Differences in the experimental preparation and methods may account for some of this inconsistency.

Numerical simulations using the bidomain model have calculated the transmembrane potential distribution during electrical stimulation through a unipolar electrode on the tissue surface (9–12). These calculations predict a large polarization near the electrode, which falls off rapidly with depth into the tissue. Experimentalists, using optical mapping to measure the transmembrane potential, observe a much smaller polarization near the electrode (5,13,14). Janks and Roth previously hypothesized that the measured polarization is weak compared to the calculated polarization because the optical signal is averaged over depth (15).

The signal detected in optical mapping experiments is essentially a distorted version of the transmembrane potential. The distortion is due to several mechanisms, including averaging over depth and lateral averaging of both the illuminating and emission light. Furthermore, Akar et al. and Poelzing et al. have observed that the falloff in the optical signal with distance r from the stimulating electrode is described by a single exponential, not the $\exp(-r/\lambda)/r$ decay predicted for the transmembrane potential from cable theory (16,17).

The optical signal recorded in an experiment should be compared to the optical signal (not the electrical signal) calculated in numerical simulations. These numerical simulations should incorporate the electrical properties and the diffuse nature of photon migration in cardiac tissue. In this article, our goal is to calculate both the transmembrane potential and optical signal arising in a three-dimensional slab of cardiac tissue during unipolar electrical stimulation and investigate the effects of the tissue optical properties on the signal. The effect of optical signal distortion will be quantified in terms of three parameters: the ratio of the peak depolarization to hyperpolarization, D_{peak}/H_{peak}, and the length constant, λ, measured parallel and perpendicular to the tissue fibers.

METHODS

The bidomain model is used to calculate transmembrane potential (V_m) and the extracellular potential (V_e) (18). This model consists of two coupled partial differential equations:

$$\nabla \cdot [(\tilde{g}_i + \tilde{g}_e)\nabla V_e] = -\nabla \cdot (\tilde{g}_i \nabla V_m) \quad (1)$$

$$\nabla \cdot (\tilde{g}_e \nabla V_e) = -\beta \left[G_m V_m + C_m \frac{\partial V_m}{\partial t} \right], \quad (2)$$

where β is the ratio of membrane surface area to tissue volume (0.3 μm^{-1}), C_m is the membrane capacitance (0.01 F/m^2), and G_m is the membrane conductance (1.65 S/m^2) (12). The intracellular and extracellular conductivity tensors, $\tilde{g}_i$ and $\tilde{g}_e$, specify the anisotropic electrical properties in each direction: $g_{ix} = g_{ex} = 0.1863\ S/m$, $g_{iy} = g_{iz} = 0.0186\ S/m$, and $g_{ey} = g_{ez} = 0.0745\ S/m$ (19). The calculation is for a passive membrane in steady state, where V_m represents the deviations of the transmembrane potential

Submitted December 14, 2007, and accepted for publication April 11, 2008.

Address reprint requests to Brad Roth, Dept. of Physics, Oakland University, Rochester, MI 48309. Tel.: 248-370-4871; Fax: 248-370-3408; E-mail: roth@oakland.edu.

Editor: Francisco Bezanilla.

0006-3495/08/08/2097/06 $2.00

doi: 10.1529/biophysj.107.127852

from rest. The myocardial fibers are straight and lie in the x direction. The edges of the tissue are sealed,

$$\frac{\partial V_m}{\partial n} = 0$$
$$\frac{\partial V_e}{\partial n} = 0, \tag{3}$$

and the boundary conditions at the electrode-tissue interface are

$$\frac{\partial V_m}{\partial n} = -\frac{\partial V_e}{\partial n} \tag{4}$$
$$V_e = V_{electrode}, \tag{5}$$

where n is the direction normal to the surface and $V_{electrode}$ is the voltage of the stimulus electrode (1 V). The cathode is centered on the upper surface, and the anode is centered on the lower surface (see Fig. 1 in Patel and Roth (11)).

The diffuse photon density due to uniform collimated illumination (Φ_{illum}) and the photon density due to voltage sensitive fluorescent emission (Φ_{em}) at all points in the three-dimensional piece of cardiac tissue are calculated using the steady-state, photon diffusion equation (20),

$$D\nabla^2\Phi(\mathbf{r}) - \mu_a\Phi(\mathbf{r}) = -S(\mathbf{r}), \tag{6}$$

where Φ is the photon density at any point in the tissue $\mathbf{r}$, D is the optical diffusion constant, μ_a is the absorption coefficient, and $S(\mathbf{r})$ describes the photon source. The diffusion constant is

$$D = \frac{1}{3(\mu_s(1-g)+\mu_a)}, \tag{7}$$

where μ_s is the scattering coefficient and g is the anisotropy coefficient (21).

The effect of uniform illumination is solved using Eq. 6 with a source term given by (20,22,23)

$$S_{illum}(z) = \mu_s' e^{-(\mu_s'+\mu_a)z}. \tag{8}$$

We will follow Flock et al. and consider an isotropic source and use the reduced scattering coefficient $\mu_s' = \mu_s(1-g)$ (22). Our standard values of the illumination optical parameters μ_s, g, and μ_a are 23.0 mm^{-1}, 0.94, and 0.52 mm^{-1}, respectively, and are taken from the optical parameters at the illumination wavelength, 488 nm, of the dye di-4-ANEPPS for rabbit myocardium (21).

The voltage-dependent fluorescent emission results from the excitation of the dye by illumination light. The photon density resulting from this voltage-dependent process is calculated using Eq. 6 with the source term, S, being given by

$$S_{em}(\mathbf{r}) = V_m(\mathbf{r})\left[\Phi_{illum}(\mathbf{r}) + e^{-(\mu_s'+\mu_a)z}\right], \tag{9}$$

where the two terms multiplying V_m are the diffuse photon density and the incident unscattered (ballistic) photon density. Our standard values of the emission optical parameters μ_s, g, and μ_a are 21.8 mm^{-1}, 0.96, and 0.1 mm^{-1}, respectively, and are consistent with those taken at 669 nm di-4-ANEPPS emission wavelength for rabbit myocardium (21).

A partial current boundary condition is used to calculate Φ_{illum} and Φ_{em} at the surface of the tissue ($z = 0$),

$$\Phi = 2D\frac{1+R_{eff}}{1-R_{eff}}\nabla\Phi\cdot\hat{n}, \tag{10}$$

where R_{eff} is the effective reflection coefficient and is dependent on the relative refractive indices of the tissue and air surface (24) and $\hat{n}$ is the unit vector normal to the tissue surface. The refractive indices of air and tissue are 1 and 1.4, respectively. The formulation of R_{eff} in Haskell et al. yields $R_{eff} = 0.49$ (24). Additionally, another boundary condition is applied to Φ_{em},

$$\frac{\partial\Phi_{em}}{\partial n} = 0, \tag{11}$$

at the edges of the tissue.

The recorded optical signal ($\Phi_{optical}$) is calculated from the photon density exiting the tissue surface by applying Fick's Law (25),

$$\Phi_{optical} = -D_{em}\nabla\Phi_{em}\cdot\hat{n}. \tag{12}$$

The detection of the optical signal from the tissue surface approximates the conditions of optical mapping experimental setups (26–30).

The solution for Φ_{illum} can be found analytically and is

$$\Phi_{illum}(z) = 3\left(\frac{1-3D_{il}\mu_{a,il}}{1-9D_{il}\mu_{a,il}}\right) \times \left[\frac{1+\frac{2}{3}\left(\frac{1+R_{eff}}{1-R_{eff}}\right)}{1+\frac{2D_{il}}{\delta}\left(\frac{1+R_{eff}}{1-R_{eff}}\right)}e^{-z/\delta} - e^{-z/3D_{il}}\right], \tag{13}$$

where $\delta = \sqrt{D_{il}/\mu_{a,il}}$ (20,23). Fig. 1 depicts Φ_{illum} as a function of depth. The length constant $\delta = 0.581$ mm, whereas $3D_{il} = 0.526$ mm. The ballistic photons also excite the dye (31), and the sum of the diffuse and ballistic photons is shown in Fig. 1.

Numerical calculations of V_m, V_e, and Φ_{em} were performed on a 10 mm × 10 mm × 10 mm slab of cardiac tissue stimulated by a cathode electrode 10 μm in diameter. The myocardial fibers are straight and lie along the x axis. The tissue is discretized with space steps $\Delta x = 0.03$ mm and $\Delta y = \Delta z = 0.012$ mm (11). At each time step, V_m is calculated using an explicit Euler method, whereas a technique of successive overrelaxation is used to calculate V_e and Φ_{em}. All simulations are run for 30 ms to allow regions of tissue away from the electrode to reach electrical steady state (12). The calculations of V_m, V_e, and Φ_{em} are made over one-eighth of the tissue by using symmetry conditions.

Optical signals calculated from Eq. 12 are normalized with respect to a calibration constant in a manner similar to experiments. The calibration constant is the optical signal one would measure when V_m is uniformly distributed throughout the tissue, for instance during the peak of the action potential. This is calculated by using a uniform V_m in the source term to solve Eq. 6. As a result of this calibration, factors such as the intensity of illumination light and the efficiency of the dye cancel out.

The length constant, λ, is calculated through least-squares fitting of V_m to $\exp(-r/\lambda)/r$, and the optical signal to $\exp(-r/\lambda)$, over a range of a

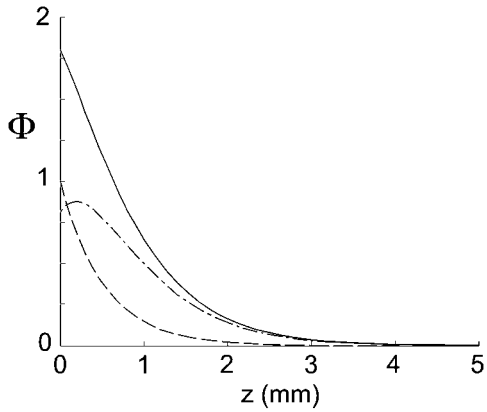

FIGURE 1 Diffuse (*dot-dashed curve*) and ballistic (*dashed*) photon density (illumination) and their sum (*solid*), as functions of depth below the tissue surface. The diffuse photon density is calculated using Eq. 13 and obeys the partial current boundary condition (Eq. 10), whereas the ballistic photons obey Beer's Law.

millimeter from the electrode. This range is consistent with optical mapping experiments, which measured the decay in the signal out to a millimeter from the electrode (16,17).

RESULTS

The transmembrane potential produced by a cathodal stimulus on one quadrant of the tissue surface is depicted in Fig. 2 *A*. This surface distribution of V_m contains a region of depolarization adjacent to a region of hyperpolarization as described by Sepulveda et al. (9). The region of depolarization is underneath the electrode and extends perpendicular to the fiber direction (y direction in Fig. 2 *A*), whereas hyperpolarization occurs on either side of the electrode and extends parallel to the fibers (x direction). The value of D_{peak}/H_{peak} in Fig. 2 *A* is 5.4×10^3. The length constant for V_m is 0.316 and 0.211 mm parallel and perpendicular to the fibers ($R^2 = 0.9998$ and 0.9992, respectively).

Fig. 2 *B* depicts the optical signal that would be detected in an optical mapping experiment due to the distribution of V_m in Fig. 2 *A*. The signal is similar to V_m: there is a region of depolarization adjacent to a region of hyperpolarization. There are two features that differ between the optical signal and V_m. First, the regions of the depolarization and hyperpolarization in the optical signal are distorted compared with those regions in V_m. The ''crossover'' region (the transition from depolarization to hyperpolarization along the x axis) occurs farther from the electrode in the optical signal. In Fig. 2, this region occurs at a point that appears gray lying between the white (depolarization) and black (hyperpolarization) regions. The value of D_{peak}/H_{peak} in Fig. 2 *B* is 56.6. The optical signal has $\lambda = 0.983$ and 0.784 mm parallel and perpendicular to the fibers ($R^2 = 0.9975$ and 0.9954, respectively).

Second, the amplitude of the optical signal near the electrode is much smaller in Fig. 2 *B* than in Fig. 2 *A* (note the different gray scales in Fig. 2). Fig. 3 shows the falloff in both the optical signal and V_m along directions parallel and perpendicular to the fibers on a semilog scale. Fig. 3 *A* shows the difference in the ''crossover'' point between the optical signal and V_m. This point occurs 0.84 mm from the electrode in the distribution of V_m, yet the optical signal shows that this region occurs 1.82 mm away. Fig. 3 *B* shows that the optical signal is larger than V_m at distances $>\sim 1$ mm from the electrode.

The distortion of optical signal is quantified by varying μ_s and μ_a over an acceptable range that is consistent with the experimental uncertainty in the data for rabbit myocardium at 488 nm and 669 nm illumination and emission wavelengths, respectively (21). Fig. 4 shows the effect of varying the optical coefficients on the measured D_{peak}/H_{peak}, and λ from the acquired optical signal. Fig. 4 *A* shows that the variation in the optical coefficients causes a deviation of 5–21% in D_{peak}/H_{peak} from the standard optical coefficients measured by Ding et al. (21). The variation of the length constants by the optical parameters is depicted in Fig. 4, *B* and *C*. The measured length constants vary by at most 11% from the standard coefficients. The results are more sensitive to $\mu_{s,em}$ than the other parameters.

Poelzing et al. and Akar et al. used optical mapping to estimate the electrical length constant, and thereby monitor the degree of cellular coupling in the tissue (16,17). To study how photon diffusion affects these recordings, we vary the electrical conductivity in the tissue and determine how these changes affect the resulting length constants measured optically. All conductivities are changed by the same factor, so the degree of anisotropy in the intracellular and extracellular spaces is constant. In the bidomain model, the electrical length constants parallel and perpendicular to the fibers are

$$\lambda_x = \sqrt{\frac{g_{ix}g_{ex}}{G_m\beta(g_{ix}+g_{ex})}} \text{ and } \lambda_y = \sqrt{\frac{g_{iy}g_{ey}}{G_m\beta(g_{iy}+g_{ey})}}. \quad (14)$$

Fig. 3 shows that the length constants calculated from the optical signal are much larger than the true electrical length constants. A decrease in the conductivity by a factor of 2 causes the optical measurement of λ_x to decrease by 23%, whereas an increase by the same amount causes λ_x to increase by 28%. Similarly, a decrease in conductivity by two caused λ_y to decrease by 23%, whereas an increase by the same amount caused an increase in λ_y by 27%. Equation 14 suggests that a factor of 2 increase in the conductivity should result in a 41% increase in λ. Thus, the optical measurement underestimates changes in cell coupling.

DISCUSSION

Our results show that the average transmembrane potential, V_m, is greatly affected by optical averaging over depth,

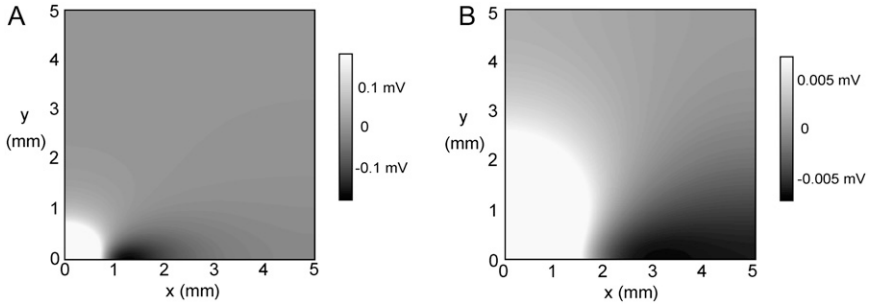

FIGURE 2 Transmembrane potential (*A*) and optical signal (*B*) due to a point electrode stimulus over one quarter of the tissue surface. The gray scale extends over the range of ± the absolute value of the peak hyperpolarization. This scale saturates under the electrode, where the depolarization is >100 mV (see Fig. 3).

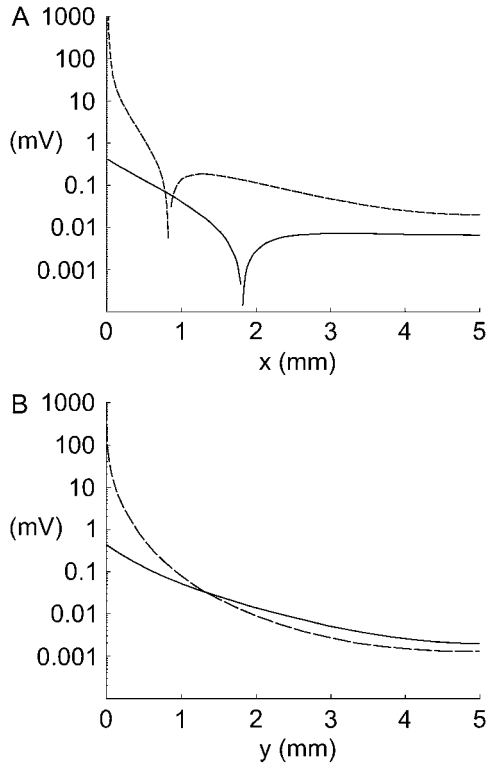

FIGURE 3 Absolute value of both the optical signal (*solid curve*) and V_m (*dashed*) versus distance from the electrode. The falloff is (*A*) parallel to and (*B*) perpendicular to the fibers.

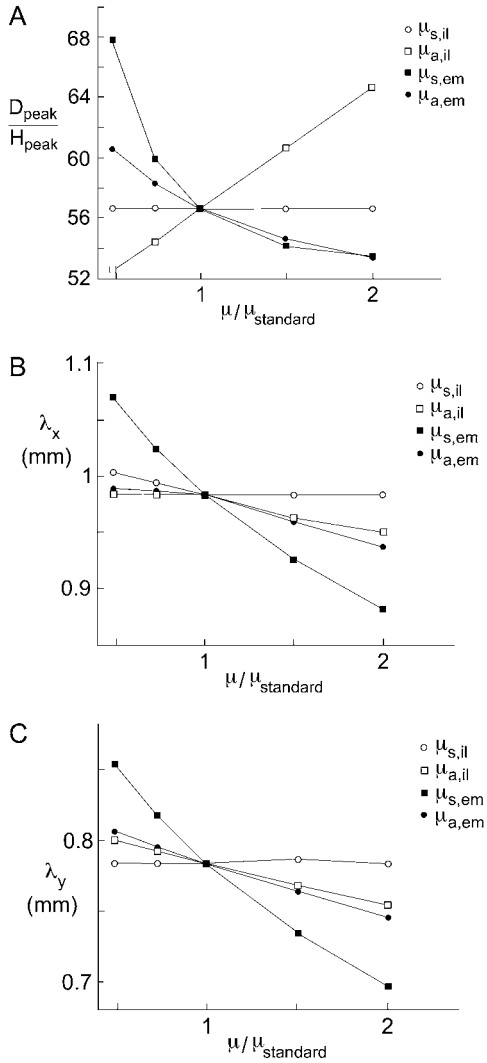

FIGURE 4 Ratio D_{peak}/H_{peak} (*A*), λ_x (parallel to fibers) (*B*), and λ_y (perpendicular to fibers) (*C*) versus variation in the optical parameters μ_s and μ_a.

consistent with previous studies (15,26,30). In general, the optical signal is a distorted version of V_m. The result is a ''flattening'' of the detected signal: the falloff of V_m with distance is reduced in the optical signal near the electrode, whereas far away the optical signal is larger than V_m. The reduction in the optical signal is consistent with the experimental measurements of Akar et al. (16), who found that ''the decay of [V_m] was well described by a single exponential.'' Although these results do not lead to a purely exponential falloff with r, the rapid falloff near the electrode caused by the $1/r$ factor in $\exp(-r/\lambda)/r$ is attenuated, giving the optical signal a more nearly exponential appearance (in Fig. 3, an exponential decay would appear as a straight line in the semilog plot).

The effect of lateral averaging can be observed where the magnitude of the optical signal is larger than V_m (Fig. 3 *B*). This effect is prevalent ~2–3 mm away from the stimulating electrode. The flat portion of the curves at 5 mm in Fig. 3, *A* and *B*, is caused by the boundary condition in Eq. 11.

The density of illuminating photons is calculated using the method described by Flock et al. (22), Hemenger (23), and Ishimaru (20). This method is different than those used by previous authors studying optical mapping of cardiac tissue (26,29,30). This problem is difficult, because it depends on the detailed assumptions of how the photons scatter. We assume an isotropic source term, with a reduced scattering coefficient, $\mu_s' = \mu_s(1-g)$. True anisotropic scattering results in an additional source term and a change to the partial current boundary condition in Eq. 10 (20). In fact, the diffusion approximation is not strictly valid for regions within a distance δ of the tissue surface. However, Flock et al. have compared the diffusion equation to Monte Carlo simulations and found the two agree well (22). Our bidomain/diffusion model simulates the effect of uniform illuminating light that is collimated. Our results would therefore not apply to experiments using a method of laser scanning for the illuminating light (3). The use of a calibrated optical signal implies that our results are independent of the illumination intensity and the efficiency of the dye.

Another technical issue is that we use a source term for the excitation process (Eq. 9) that includes both diffuse and ballistic photons during the illumination process. Recently, Roth investigated the effect of including both diffuse and ballistic photons during illumination, and found that consid-

ering only the effect of diffuse photons causes an incorrect estimation of the falloff in the density of photons with depth (31).

A third technical issue is the discrepancy between our calculations of the electrical length constants and those from cable theory. In the bidomain model, the electrical length constant, given by Eq. 14, is 0.434 and 0.174 mm, and simulations of our bidomain/diffusion model with equal anisotropy ratios give length constants of 0.443 and 0.177 mm (a variation of 2% or less from the nominal values, reflecting our numerical error). However, when the tissue has unequal anisotropy ratios, the length constants that we predict for V_m are 0.316 and 0.211 mm. Apparently, for unequal anisotropy ratios, V_m does not fall off with the length constant given by a one-dimensional cable model.

In a previous study, Janks and Roth calculated the effect of optical averaging over depth by using an exponential decay of the light intensity (15). We performed a similar simulation in which we considered only averaging over depth in our calculation (Fig. 5). Near the electrode, the magnitude of the signal obtained by averaging over depth is 1–2 orders of magnitude smaller than V_m, and the spatial distribution of this signal is similar to that of V_m. In contrast, the spatial distribution of the optical signal calculated from the bidomain/diffusion model is a distorted version of V_m. Janks and Roth apparently underestimated the impact of scattering on the optical signal (15).

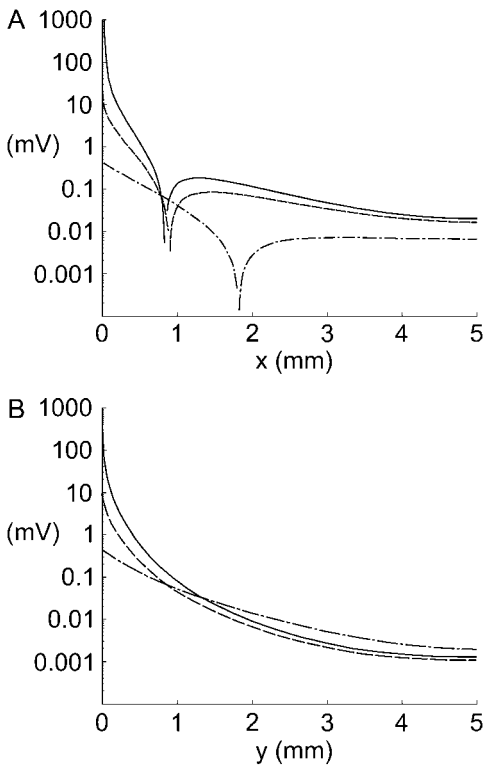

FIGURE 5 Absolute value of V_m (*solid curve*), the optical signal (*dash-dot*), and the optical signal due to the effect of averaging over depth only with no lateral averaging (*dash*) versus distance from the electrode. The falloff is (*A*) parallel to and (*B*) perpendicular to the fibers.

We analyze a steady-state model that neglects fiber rotation with depth, fiber curvature, tissue heterogeneities, and electroporation. Additionally, we do not account for other factors such as depth of focus and averaging over a finite pixel size (21). Furthermore, we assume that the membrane dye responds linearly to changes in V_m, an assumption that may not hold for large polarizations (32). The membrane model we have used represents a passive, linear resistance, which may not be appropriate for large polarizations (33). Measured magnitudes of V_m typically fall inside the range of 0.02–200 mV. The bidomain/diffusion model is linear, so our results should be appropriately scaled to conform to typical experimental ranges but would not otherwise change. In many experiments, noise significantly reduces the ability to measure accurately the optical signal farther than a millimeter from the stimulating electrode, which was a major consideration in calculating λ. These issues, in addition to others, need to be considered when comparing experimental results to numerical simulations (34).

Does a bidomain/diffusion model improve the agreement between optical measurements and numerical predictions? Our results suggest that a three-dimensional bidomain/diffusion model can resolve the discrepancy between a small V_m that is measured experimentally and the potential calculated numerically (34). Additionally, the model predicts an optical signal that decays like a simple exponential, $\exp(-r/\lambda)$, with distance from the stimulus electrode, which agrees with the experimental findings of Akar et al. and Poelzing et al. (16,17). Thus, when experimentalists try to predict V_m, they should compare their results to the optical signal calculated from a three-dimensional bidomain/diffusion model. Imaging methods using the signals from optical mapping experiments will need to account for these distortions to accurately reconstruct the transmembrane potential (29).

This research was supported by the Research Excellence Fund at Oakland University.

REFERENCES

1. Roth, B. J., and W. Krassowska. 1998. The induction of reentry in cardiac tissue. The missing link: How electric fields alter transmembrane potential. *Chaos*. 8:204–220.
2. Rosenbaum, D. S., and J. Jalife. 2001. Optical Mapping of Cardiac Excitation and Arrhythmias. Futura, Armonk, NY.
3. Knisley, S. B., B. C. Hill, and R. E. Ideker. 1994. Virtual electrode effects in myocardial fibers. *Biophys. J.* 66:719–728.
4. Gray, R. A. 1999. What exactly are optically recorded 'action potentials'? *J. Cardiovasc. Electrophysiol.* 10:1463–1466.
5. Knisley, S. B. 1995. Transmembrane voltage changes during unipolar stimulation of rabbit ventricle. *Circ. Res.* 77:1229–1239.
6. Girouard, S. D., K. R. Laurita, and D. S. Rosenbaum. 1996. Unique properties of cardiac action potentials recorded with voltage-sensitive dyes. *J. Cardiovasc. Electrophysiol.* 7:1024–1038.
7. Al-Khadra, A., V. Nikolski, and I. R. Efimov. 2000. The role of electroporation in defibrillation. *Circ. Res.* 87:797–804.
8. Baxter, W. T., S. F. Mironov, A. V. Zaitsev, J. Jalife, and A. M. Pertsov. 2001. Visualizing excitation waves inside cardiac muscle using transillumination. *Biophys. J.* 80:516–530.

9. Sepulveda, N. G., B. J. Roth, and J. P. Wikswo, Jr. 1989. Current injection into a two-dimensional anisotropic bidomain. *Biophys. J.* 55: 987–990.

10. Roth, B. J. 1995. A mathematical model of make and break electrical stimulation of cardiac tissue by a unipolar anode or cathode. *IEEE Trans. Biomed. Eng.* 42:1174–1184.

11. Patel, S. G., and B. J. Roth. 2000. How electrode size affects the electric potential distribution in cardiac tissue. *IEEE Trans. Biomed. Eng.* 47:1284–1287.

12. Latimer, D. C., and B. J. Roth. 1998. Electrical stimulation of cardiac tissue by a bipolar electrode in a conductive bath. *IEEE Trans. Biomed. Eng.* 45:1449–1458.

13. Neunlist, M., and L. Tung. 1995. Spatial distribution of cardiac transmembrane potentials around an extracellular electrode: Dependence on fiber orientation. *Biophys. J.* 68:2310–2322.

14. Wikswo, J. P., Jr., S.-F. Lin, and R. A. Abbas. 1995. Virtual electrodes in cardiac tissue: A common mechanism for anodal and cathodal stimulation. *Biophys. J.* 69:2195–2210.

15. Janks, D. L., and B. J. Roth. 2002. Averaging over depth during optical mapping of unipolar stimulation. *IEEE Trans. Biomed. Eng.* 49:1051–1054.

16. Akar, F. G., B. J. Roth, and D. S. Rosenbaum. 2001. Optical measurement of cell-to-cell coupling in intact heart using subthreshold electrical stimulation. *Am. J. Physiol.* 281:H533–H542.

17. Poelzing, S., B. J. Roth, and D. S. Rosenbaum. 2005. Optical measurements reveal nature of intercellular coupling across ventricular wall. *Am. J. Physiol.* 289:H1428–H1435.

18. Henriquez, C. S. 1993. Simulating the electrical behavior of cardiac tissue using the bidomain model. *Crit. Rev. Biomed. Eng.* 21:1–77.

19. Roth, B. J. 1997. Electrical conductivity values used with the bidomain model of cardiac tissue. *IEEE Trans. Biomed. Eng.* 44:326–328.

20. Ishimaru, A. 1997. Wave Propagation and Scattering in Random Media. IEEE Press, Piscataway, NJ.

21. Ding, L., R. Splinter, and S. B. Knisley. 2001. Quantifying spatial localization of optical mapping using Monte Carlo simulations. *IEEE Trans. Biomed. Eng.* 48:1098–1107.

22. Flock, S. T., M. S. Patterson, B. C. Wilson, and D. R. Wyman. 1989. Monte Carlo modeling of light propagation in highly scattering tissue—I: Model predictions and comparison with diffusion theory. *IEEE Trans. Biomed. Eng.* 36:1162–1168.

23. Hemenger, R. P. 1977. Optical properties of turbid media with specularly reflecting boundaries: Applications to biological problems. *Appl. Opt.* 16:2007–2012.

24. Haskell, R. C., L. O. Svaasand, T.-T. Tsay, T.-C. Feng, M. S. McAdams, and B. J. Tromberg. 1994. Boundary conditions for the diffusion equation in radiative transfer. *J. Opt. Soc. Am. A Opt. Image Sci. Vis.* 11:2727–2741.

25. Hyatt, C. J., S. F. Mironov, M. Wellner, O. Berenfeld, A. K. Popp, D. A. Weitz, J. Jalife, and A. M. Pertsov. 2003. Synthesis of voltage-sensitive fluorescence signals from three-dimensional myocardial activation patterns. *Biophys. J.* 85:2673–2683.

26. Bishop, M. J., B. Rodriguez, J. Eason, J. P. Whiteley, N. Trayanova, and D. J. Gavaghan. 2006. Synthesis of voltage-sensitive optical signals: Application to panoramic optical mapping. *Biophys. J.* 90:2938–2945.

27. Lin, S.-F., and J. P. Wikswo, Jr. 1999. Panoramic optical imaging of electrical propagation in isolated heart. *J. Biomed. Opt.* 4:200–207.

28. Efimov, I., V. Sidorov, Y. Cheng, and B. Wollenzier. 1999. Evidence of three-dimensional scroll waves with ribbon-shaped filaments as a mechanism of ventricular tachycardia in the isolated rabbit heart. *J. Cardiovasc. Electrophysiol.* 10:1452–1462.

29. Bernus, O., M. Wellner, S. F. Mironov, and A. M. Pertsov. 2005. Simulation of voltage-sensitive optical signals in three-dimensional slabs of cardiac tissue: Application to transillumination and coaxial imaging methods. *Phys. Med. Biol.* 50:215–229.

30. Bishop, M. J., B. Rodriguez, F. Qu, I. R. Efimov, D. J. Gavaghan, and N. A. Trayanova. 2007. The role of photon scattering in optical signal distortion during arrhythmia and defibrillation. *Biophys. J.* 93:3714–3726.

31. Roth, B. J. 2008. Photon density measured over a cut surface: Implications for optical mapping of the heart. *IEEE Trans. Biomed. Eng.* In press.

32. Cheng, D. K.-L., L. Tung, and E. A. Sobie. 1999. Nonuniform responses of transmembrane potential during electric field stimulation of single cardiac cells. *Am. J. Physiol.* 277:H351–H362.

33. Cheek, E. R., R. E. Ideker, and V. G. Fast. 2000. Nonlinear changes of transmembrane potential during defibrillation shocks. *Circ. Res.* 87: 453–459.

34. Roth, B. J. 2002. Artifacts, assumptions, and ambiguity: Pitfalls in comparing experimental results to numerical simulations when studying electrical stimulation of the heart. *Chaos.* 12:973–981.